Turkish Journal of Engineering

Turkish Journal of Engineering (TUJE)
Vol. 3, Issue 1, pp. 43-50, January 2019
ISSN 2587-1366, Turkey
DOI: 10.31127/tuje.452865
Research Article

COMPARISON OF EFFECT OF NICKEL CONCENTRATION ON CRYSTALLOGRAPHIC STRUCTURE AND MORPHOLOGY OF ZINC OXIDE NANOPOWDERS

Saadet Yıldırımcan [1] and Selma Erat *[2,3]

[1] Toros University, Faculty of Engineering, Department of Electrical-Electronics Engineering, Mersin, Turkey
ORCID ID 0000 – 0002 – 9044 – 6908
saadetyildirimcan@gmail.com

[2] Mersin University, Vocational School of Technical Sciences, Department of Medical Services and Techniques, Program of Opticianry, Mersin, Turkey
[3] Advanced Technology, Research and Application Center, Mersin University, Mersin, Turkey
ORCID ID 0000 – 0001 – 7187 – 7668
selmaerat33@gmail.com

* Corresponding Author
Received: 10/08/2018 Accepted: 11/09/2018

ABSTRACT
In this study, we work on the effect of Ni doping on the crystallographic structure, morphology, and optical properties of ZnO nanoparticles. ZnO and Ni doped ZnO nanopowders were synthesized by sol-gel technique with different Ni concentration (5%, 10%, and 15%). The crystallographic structure was characterized by conventional X-ray Diffraction (XRD) technique. The results confirm that Ni doping does not change the single hexagonal phase existing in pure ZnO whereas in high Ni doping concentration (10% and 15%) causes to grow a secondary phase due to presence of NiO. FE-SEM, EDX, FTIR techniques are used for morphology, elemental, and chemical analyses of the samples. Optical properties of the samples are investigated by using UV-VIS spectrophotometer.

Keywords: *ZnO, Nickel, Crystallographic Structure, Morphology, Optical Properties*

1. INTRODUCTION

Recently, zinc oxide (ZnO) being a member of II-VI group has attracted much attention due to its potential applications in diverse fields (Vijayaprasath *et al.*, 2016; Kittilstved *et al.*, 2006). For instance, ZnO with a direct wide-band gap (in bulk form, 3.37 eV at 300 K), large exciton binding energy (60 meV), remarkable piezoelectric, electro-optic properties, and great chemical stability, (Bappaditya *et al.*, 2015; Dietl, 2007; Pearton *et al.*, 2005) has received eminent attention for its electronic and photonic applications (Yildirimcan *et al.*, 2016) such as photodetectors (Kind *et al.*, 2002), photodiodes (Lee *et al.*, 2002), light emitting diodes (Saito *et al.*, 2002), surface acoustic wave filters (Emanetoglu *et al.*, 1999), photonic crystals (Chen *et al.*, 2000), optical modulator waveguides (Koch *et al.*, 1995), room-temperature ultraviolent (UV) lasers (Huang *et al.*, 2001), gas sensors (Mitra *et al.*, 1998; Godavarti *et al.*, 2017), and solar cells and flat panel displayers (Law *et al.*, 2005; Martinson *et al.*, 2007; Shoushtari *et al.*, 2017; El-Hilo *et al.*, 2009; Ellmer *et al.*, 2008).

It is known that the physical properties of nanosized materials are greatly affected by their size and shape (Romeiro *et al.*, 2015). There are several methods to synthesize nanoparticles. Some of the methods to prepare ZnO nanoparticles are in following: microwave-assisted synthesis (Schneider *et al.*, 2010), wet chemical (Toloman *et al.*, 2013), hydrothermal synthesis (Li *et al.*, 2001), aerosol spray analysis (Motaung *et al.*, 2014), hydrolysis condensation (Cohn *et al.*, 2012), and sol-gel processing (Bahnemann *et al.*, 1987). Doping ZnO with transition metal (TM) such as Cr, Fe, Co, Mn, or Ni results in some important changes in microstructure and further in physical properties such as optical, electrical, and magnetic properties. It is expected that Ni^{2+} ion thanks to its smaller ionic radius (0.55 Å) compared to Zn^{2+} (0.60 Å) (Bappaditya *et al.*, 2015) have a larger solubility in ZnO, which is mostly crystallized in hexagonal wurtzite structure (mainly with 110 preferred orientation) with tetrahedrally coordinated O^{2-} and Zn^{2+} ions (Samanta *et al.*, 2018). It was reported that the chemical stability on Ni^{2+} ion upon occupying Zn^{2+} sites, makes it unique and identifies it as one of the most efficient doping element because it enhances ZnO with optical and electrical properties (Fabbiyola *et al.*, 2017; Raja *et al.*, 2014).

There are also some other studies about Ni doped ZnO using sol-gel method (Srinet *et al.*, 2013; Liu *et al.*, 2014), low temperature hydrothermal method (Xu *et al.*, 2016), low temperature wet chemical method (Rana *et al.*, 2016) and about shape controlled magnetic nanoplatelets of Ni doped ZnO (Jadhav *et al.*, 2016). The crystallographic structure and morphology of Ni doped ZnO, and further physical properties, are affected by preparation technique and external conditions such as concentration of Ni, reaction temperature, reaction time, annealing temperature, pH value, starting precursors, solution concentration, and etc.

In this study, ZnO nanopowders doped with different Ni concentration were synthesized by sol-gel technique using zinc nitrate hexahydrate ($Zn(NO_3)_2.6H_2O$) and nickel nitrate hexahydrate ($Ni(NO_3)_2.6H_2O$) at pH value of 10. The samples were annealed at 500°C for 2h. The crystallographic structure of the samples was investigated by conventional x-ray diffraction (XRD) technique and morphology of the samples was investigated by field emission-scanning electron microscopy (FE-SEM) along with elemental analysis by energy dispersive x-ray (EDX). Besides, Fourier transform infrared spectroscopy (FTIR) technique is used to analyse the chemical bonding and constituting elements of the samples. Further, the optical properties of Ni doped ZnO nanopowders were investigated by using UV-VIS spectrometer and the results were presented in detail.

2. EXPERIMENTAL PROCESS

ZnO and Ni doped ZnO nanopowders were prepared by using sol-gel technique. The zinc nitrate hexahydrate ($Zn(NO_3)_2.6H_2O$, Acros Organics), nickel nitrate hexahydrate ($Ni(NO_3)_2.6H_2O$, Sigma Aldrich, for Ni doped ZnO), polyethylene glycol (PEG300, Aldrich Chemistry) and ammonia (NH_3, Analar Normapur) were used as precursors. As a first step, 2.97 g of $Zn(NO_3)_2.6H_2O$ was dissolved in 100 mL of distilled water (Yildirimcan *et al.*, 2016). As a second step, 3.36 g PEG300 was added into the existing solution. The pH of the solution was adjusted to 10 by using ammonia (NH_3). The resulting solution was mixed overnight at 80°C using a magnetic stirrer to get a homogeneous solution in which precipitates were visible. Then, the water in the final solution was evaporated at 100°C. Finally, the precipitate was annealed at 500°C for 2 h. The similar procedure was followed in order to produce Ni doped ZnO nanopowders. $Ni(NO_3)_2.6H_2O$ was dissolved in distilled water at certain ratios. The prepared Ni solution was added into the pure ZnO precursor solution at stoichiometric ratios, 5%, 10% and 15%. Also, Ni doped ZnO nanopowders were produced at pH=10 and annealed at 500°C for 2 h.

The crystallographic structure of the samples were investigated by using x-ray diffraction (XRD) (Bruker D8 Advanced Series powder diffractometer) (40 kV, 40 mA, Cu$K\alpha$ λ=1.5405 Å) in steps of 0.02° in the rage of $20° \leq 2\theta \leq 85°$. Field emission-scanning electron microscopy (FE-SEM) (Zeiss/Supra 55 FE-SEM) was used in order to determine the morphology of the samples. The Zeiss/Supra 55 FE-SEM was equipped with an energy dispersive x-ray spectrometer, which was used to record the EDX diffractogram for elemental analysis. Fourier transform infrared (FTIR) spectra were recorded by using Perkin Elmer spectrometer with ATR unit in order to analyse the chemical bonding and constituting elements of the samples.

3. RESULTS AND DISCUSSIONS

Structural, elemental and morphological analyzes along with determination of optical properties were made in detail and results were presented in the individual parts in following. The results were compared with literature and discussed.

3.1. Structural Analysis of the ZnO and ZnO:Ni Nanoparticles

It is known that the possible growth mechanism of the nanomaterials can be described on basis of chemical

reactions and nucleation process (Rana *et al.*, 2016). The possible chemical reactions, which are responsible for the growth on Ni doped ZnO nanostructure were already given in (Rana *et al.*, 2016). The XRD diffraction patterns of the pure ZnO and Ni doped ZnO nanopowders synthesized by sol-gel technique are shown in Fig. 1(a), enlarged in Fig. 1(b), respectively.

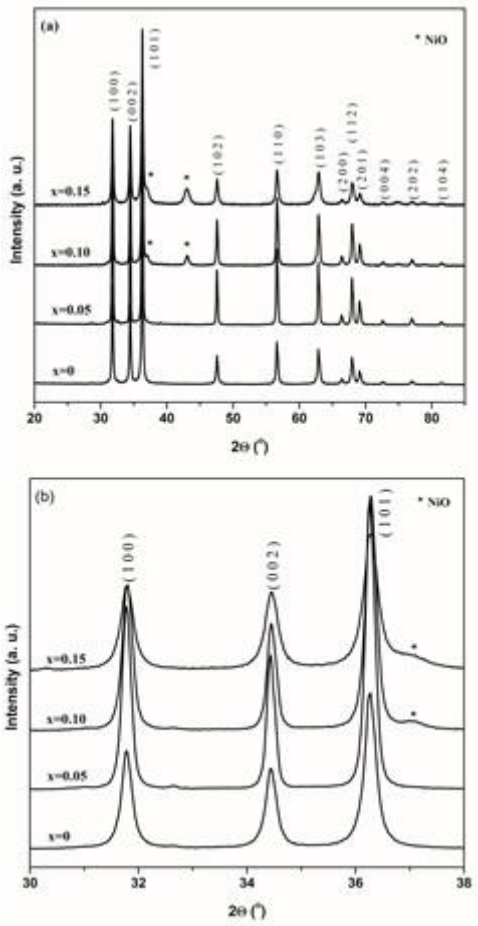

Fig. 1. (a) X-ray diffraction patterns for Ni doped ZnO nanocrystals depending on Ni concentration; (b) expanded view of (100), (002) and (101) peaks in all of the samples

The sharp peaks in Fig. 1 are evidence that pure and Ni doped ZnO nanoparticles are well crystallized. Pure ZnO exhibits a hexagonal phase of wurtzite type with (101) preferred growth direction and it is phase pure, which means no extra peaks, are observed. In other word, all the major diffraction peaks for the sample x=0 can be perfectly indexed with pure ZnO (phase: hexagonal, lattice: primitive, JCPDS 036-1451). Doping ZnO with different Ni concentration does not change the hexagonal phase. However, for the samples with x=0.10 and x=0.15 a secondary phase is observed. The diffraction peaks occurred at 2θ=37.01° and 2θ=43.09° are attributed to presence of NiO (JCPDS 004-0835). This is in agreement with the literature (Srinet *et al.*, 2013) in which a secondary phase is observed for Ni concentration of 6%. Our sample with x=0.05 prepared with sol-gel technique is phase pure whereas it was observed in literature that the sample with x=0.05 prepared with ball milling technique existed a secondary phase due to NiO/Ni (Bappaditya *et al.*, 2015). The lattice parameters (*a*, *c*) of pure and Ni doped ZnO nanopowders were calculated using the XRD data with the help of Bragg Law

$$2dsin\theta = n\lambda \quad (1)$$

(*n*=1; λ is the wavelength of incident X-ray used) and following formula, which is defined for hexagonal phase:

$$\frac{1}{d^2} = \frac{4}{3}\left[\frac{h^2+hk+k^2}{a^2}\right] + \frac{l^2}{c^2} \quad (2)$$

where *d* is the distance between two different planes and (*hkl*) are the Miller indexes (Yildirimcan *et al.*, 2016). The calculation of *a*, *c* and *d* were made with respect to (100), (002), (101) diffraction peaks and then average values were calculated and the values were given in Table 1.

Table 1. Lattice parameters of *a*, *c*, and *d* of the pure ZnO and Ni doped ZnO

Sample	*a* (Å)	*c* (Å)	*d* (Å)
x=0	3.2235	5.2640	2.6299
x=0.05	3.2238	5.2645	2.6302
x=0.10	3.2228	5.2628	2.6293
x=0.15	3.2232	5.2634	2.6296

Note: x is mol of Ni concentration.

The average crystallite sizes of pure and Ni doped ZnO nanopowders are calculated by applying Debye-Scherrer formula:

$$D_{hkl} = \frac{K\lambda}{\beta\cos\theta} \quad (3)$$

where *D* is the average crystallite size, β is the full width half maximum (FWHM) of the 2θ peak (100), *K* is the shape factor of the particles (used as 0.9), θ is the Bragg angle, λ is the wavelength of incident X-ray used.

The calculated crystallite size, dislocation density, and strain of pure ZnO and Ni doped ZnO nanopwders are listed in Table 2. The FWHM (β $x10^{-3}$)(rad) values are 3.799, 3.473, 3.850, and 4.616 for the samples with x=0, x=0.05, x=0.10, and x=0.15, respectively.

Table 2. Crystallite size, dislocation density, strain of pure ZnO and Ni doped ZnO nanopowders

Sample	Crystallite size (nm)	Dislocation density ($x10^{-4}$ lines/nm^2)	Strain ($x10^{-4}$)
x=0	37.93	6.950	9.135
x=0.05	41.50	5.808	8.351
x=0.10	37.43	7.138	9.257
x=0.15	31.20	10.262	11.10

Note: Calculations were made with respect to (100) peak of XRD. x is mol of Ni concentration.

The crystallite size is increased from 37.93 nm to 41.50 nm with 5% Ni doping into ZnO, which is also

confirmed by (Vignesh *et al.*, 2014). However, for higher Ni doping causes a decrease in the crystallite size for example it is 37.43 nm for the sample with x=0.10 and 31.20 nm for x=0.15. There is no linear correlation between concentration of Ni and crystallite size of the samples. This situation was concluded in the literature (Rana *et al.*, 2016) that the reason might be dissimilar conditions for different doping concentration as well as a lot of distortions in the host ZnO lattice that turns out lattice relaxation or compression in the host lattice because of the vacancy and/or interstitial defect already existing in the host lattice. The sample with x=0.05 having the highest crystallite size showing the smallest dislocation density and the smallest strain.

3.2. Elemental Analysis of the ZnO and Ni:ZnO Nanoparticles

The EDX diffractogram of pure ZnO and Ni doped ZnO are shown in Fig. 2. The diffractogram confirm the presence of the elements Zn, Ni, and O, and no other impurities in the samples. The peaks labeled as platinum (Pt), and palladium (Pd) are due to surface coating materials. The weight and atomic ratio of the samples obtained by EDX are given in Table 3.

Table 3. EDX elemental analysis of ZnO and Ni doped ZnO nanopowders

Sample	Element	Weight (%)	Atomic (%)
x=0	Zn	67.52	50.37
	Ni	-	-
	O	14.51	44.23
x=0.05	Zn	75.38	52.81
	Ni	0.50	0.39
	O	15.52	44.45
x=0.10	Zn	62.41	43.00
	Ni	5.00	3.84
	O	17.38	48.95
x=0.15	Zn	50.46	34.58
	Ni	12.79	9.76
	O	17.31	48.48

Note: x is mol of Ni concentration.

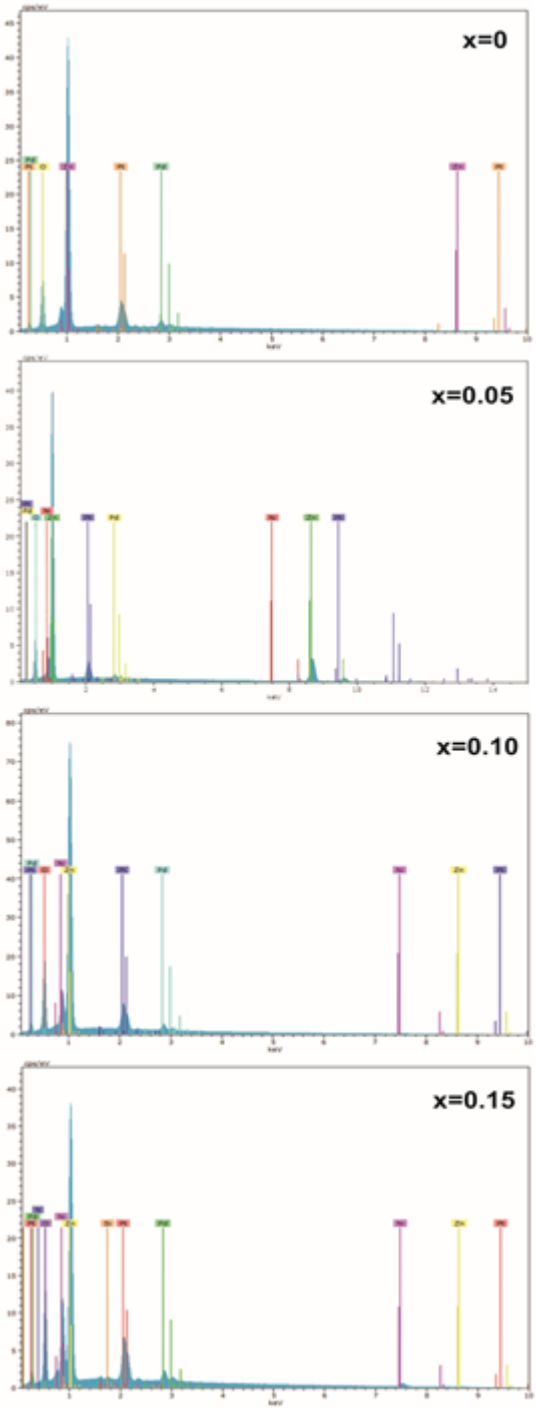

Fig. 2. EDX diffractogram of pure ZnO and Ni doped ZnO. x is mol of Ni concentration.

3.3. FT-IR Analysis of the ZnO and Ni:ZnO Nanoparticles

The chemical bonding of the nanopowders can be analyzed by using FTIR spectroscopy. Thus, FTIR spectra of pure ZnO and Ni doped ZnO were recorded in order to study the composition and chemical structure of the samples in the wave number range of 400-4000 cm^{-1} at room temperature. Fig. 3 shows the comparison of the transmittance of the samples.

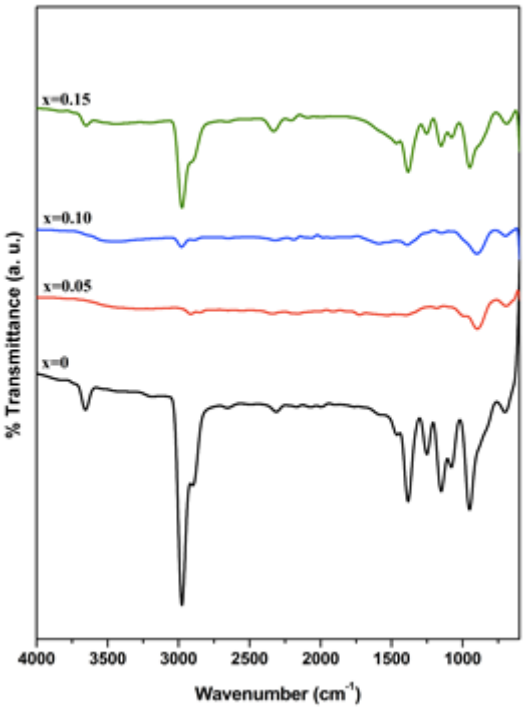

Fig. 3. FTIR spectra of pure ZnO and Ni doped ZnO. x is mol of Ni concentration.

The observed band at 3656 cm^{-1} which is quite dominant for the sample x=0 compared to the others is corresponded to stretching vibration of H_2O. It was already mentioned that the FTIR peaks at 3500-3800 cm^{-1} (both) were corresponded to stretching vibration of H_2O (Yildirimcan *et al.*, 2016). The observed bands at 2982 cm^{-1} and 2889 cm^{-1} are due to the symmetric and asymmetric $–CH_2$ stretching modes. The vibration bands between 2300 cm^{-1} and 2400 cm^{-1}, which are at 2316 cm^{-1} in the present study, were assigned to the CO_2 mode in air (Yildirimcan *et al.*, 2016). The peak at 1382 cm^{-1} is corresponded to the symmetric C=O stretching vibration modes (Samanta *et al.*, 2018). The peak at 1075 cm^{-1} is ascribed to bending vibrations of –OH groups and the peak at 946 cm^{-1} is attributed to symmetric stretching vibrations of NO_3^{-1} ions.

3.4. Microstructure Analysis of ZnO and Ni:ZnO Nanoparticles

The surface morphologies of ZnO and Ni doped ZnO nano particles are investigated by FE-SEM (see Fig. 4). It is observed that pure ZnO is composed of closely packed spherical nanoparticles. Once ZnO is doped with 5% Ni, nanorods start to exist along with spherical nanoparticles. These nanorods are not homogenous in another word, the sample with x=0.05 includes nanorods having the length ranging from nanometer to micrometer. The nanorod structure becomes more like nanoneedle once the Ni concentration is increased upto x=0.10. Besides, agglomerated nanoparticles still exist in the sample. On the other hand, nanorods mostly disappeared agglomerated spherical nanoparticles becomes dominant. The agglomeration of Ni doped ZnO was also observed in the literature (Vignesh *et al.*, 2014).

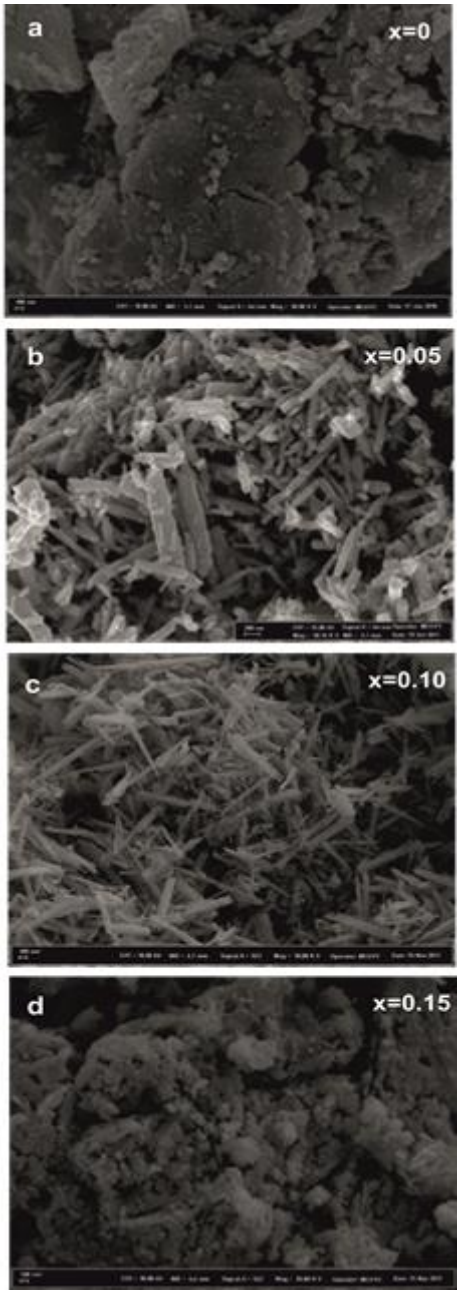

Fig. 4. SEM pictures of a) pure ZnO, b) x=0.05, c) x=0.10, d) x=0.15, x is mol of Ni concentration

3.5. Optical properties of ZnO and Ni:ZnO Nanoparticles

Fig. 5 shows the absorbance spectra of pure and Ni-doped ZnO nanoparticles. The sample doped 5% Ni shows the highest intensity.

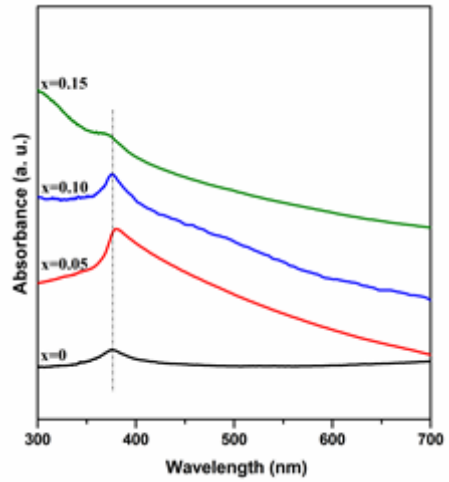

Fig. 5. Absorbance spectra of pure ZnO and Ni doped ZnO. x is mol of Ni concentration

The absorbance peaks appear in the range of 350- 400 nm. While the absorbance peak increases as doping 5% Ni^{2+}, it decreases as doping 10% and 15% Ni^{2+}, respectively. The absorption peak (known as excitonic absorption peak) of pure ZnO and Ni doped ZnO (5%, 10% and 15%) nanoparticles were observed in the wavelength around 376 nm, 380 nm, 375 nm and 370 nm, respectively. The absorption peak of pure ZnO is shifted to higher wavelength once ZnO is doped with 5% Ni similar to (Jadhav *et al.*, 2016). It is also mentioned in the literature (Guruvammal *et al.*, 2016) that one reason for red shift could be the sp-d exchange interactions between the band electrons and the localized d-electrons of the Ni^{2+} ions. However, blue shift is observed for higher Ni doping concentrations (10% and 15%). The absorption blue shift is explained by Burstein-Moss effect (Samanta *et al.*, 2018; Fabbiyola *et al.*, 2017; Rajakarthikeyan *et al.*, 2017)

4. CONCLUSIONS

The effects of Ni doping concentration on the physical properties such as structural, morphological, and optical properties of ZnO nanoparticles prepared by sol-gel technique have been investigated. Because of its smaller ionic radius compared to Zn^{2+}, the Ni^{2+} have a larger solubility in ZnO. However, there is a solubility limit: the sample with x=0.05 shows pure hexagonal phase whereas x=0.10 and x=0.15 show a secondary phase due to existing of NiO. The elemental and chemical analysis have been done by EDX and FTIR and given in parts of 3.2 and 3.3, respectively. The sample with x=0.05 has the highest crystallite size (41.50 nm) and the smallest dislocation density and following the smallest strain. The sample includes both spherical nanoparticles and nanorods ranging the length from nanometer to micrometer whereas pure ZnO includes only agglomerated spherical nanoparticles. The nanorods change into the form of nanoneedles which are deteriorated for the sample x=0.10. Nanorods or nanoneedles are mostly disappeared in the sample with x=0.15. Optical properties of the samples have been studied and the absorbance peaks are found to be at 376 nm, 380 nm, 375 nm, and 370 nm for the sample with x=0, x=0.05, x=0.10, and x=0.15, respectively.

REFERENCES

Bahnemann, D. W., Kormann, C. and Hoffmann M. R. (1987). "Preparation and characterization of quantum size zinc oxide: a detailed spectroscopic study." *J. Phys. Chem*., Vol. 91, No. 14, pp. 3789-3798.

Bappaditya P., Sarkar, D. and Giri, P. K. (2015). "Structural, optical, and magnetic properties of Ni doped ZnO nanoparticles: Correlation of magnetic moment with defect density." *Applied Surface Science*, Vol. 356, pp. 804-811.

Chen, Y. F., Bagnall, D. and Yao, T. F. (2000). "ZnO as a novel material for the UV region." *Mater. Sci. Eng. B*, Vol. 75, pp. 190-198.

Cohn, A.W., Kittilstved, K. R. and Gamelin, D. R. (2012). "Tuning the Potentials of "Extra" Electrons in Colloidal n-Type ZnO Nanocrystals via Mg^{2+} Substitution." *J. Am. Chem. Soc*., Vol. 134, No. 18, pp. 7937-7943.

Dietl, T., (2007). "Origin of ferromagnetic response in diluted magnetic semiconductors and oxides." *J. Phys.: Condens. Matter*, Vol. 19 No. 16, pp. 165204.

El-Hilo, M., Dakhel, A. A. and Ali-Mohamed, A.Y. (2009). "Room temperature ferromagnetism in nanocrystalline Ni-doped ZnO synthesized by co-precipitation." *J. Magn. and Magn. Mater*., Vol. 321 No. 14, pp. 2279-2283.

Ellmer, K., Klein, A. and Rech, B. (2008). *Transparent conductive zinc oxide – Basics and applications in thin film solar cells*, Springer Series in Materials Science, Germany.

Emanetoglu, N. W., Gorla, C., Liu, Y., Liang, S. and Lu, Y. (1999). "Epitaxial ZnO piezoelectric thin films for saw filters." *Mater. Sci. Semicond. Process*., Vol. 2, No. 3, pp. 247–252.

Fabbiyola, S., Sailaja, V., John Kennedy, L., Bououdina, M. and Judith Vijaya, J. (2017). "Optical and magnetic properties of Ni-doped ZnO nanoparticles." *Journal of Alloys and Compounds*, Vol. 694, pp. 522-531.

Godavarti, U., Mote, V. D. and Dasari, M. (2017). "Precipitated nickel doped ZnO nanoparticles with enhanced low temperature ethanol sensing properties." *Modern Electronic Materials*, Vol. 3, pp. 179-185.

Guruvammal, D., Selvaraj, S. and Meenakshi Sundar, S. (2016). "Effect of Ni-doping on the structural, optical and magnetic properties of ZnO nanoparticles by solvothermal method." *Journal of Alloys and Compounds*, Vol. 682, pp. 850-855.

Huang, M. H., Mao, S., Feick, H., Yan, H. Q., Wu, Y. Y., Kind, H., Weber, E., Russo, R. and Yang, P. D. (2001). "Room-temperature ultraviolet nanowire nanolasers." *Science*, Vol. 292, pp. 1897-1899.

Jadhav, J. and Biswas, S. (2016). "Shape-controlled

magnetic nanoplatelets of Ni-doped ZnO synthesized via a chemical precursor." *Journal of Alloys and Compounds*, Vol. 664, pp. 71-82.

Kind, H., Yan, H. Q., Messer, B., Law, M. and Yang, P. D. (2002). "Nanowire Ultraviolet Photodetectors and Optical Switches." *Adv. Mater*., Vol. 14, pp.158.

Kittilstved, K. R., Liu, W. K. and Gamelin, D. R. (2006). "Electronic structure, origins of polarity-dependent high-TC ferromagnetism in oxide-diluted magnetic semiconductors." *Nat. Mater*., Vol. 5, pp. 291-297.

Koch, M. H., Timbrell, P. Y. and Lamb, R. N. (1995). "The influence of film crystallinity on the coupling efficiency of ZnO optical modulator waveguides." Semicond. Sci. Technol., Vol. 10, pp. 1523-1527.

Law, M., Greene, L. E., Johnson, J. C., Saykally, R. and Yang, P. D. (2005). "Nanowire dye-sensitized solar cells." *Nat. Mater*., Vol. 4, pp. 455-459.

Lee, J. Y., Choi, Y. S., Kim, J. H., Park M. O., Im, S. (2002). "Optimizing n-ZnO/p-Si heterojunctions for photodiode applications." *Thin Solid Films*, Vol. 403, pp. 553-557.

Li, W. J., Shi, E. W., Zheng, Y. Q. and Yin, Z. W. (2001). "Hydrothermal preparation of nanometer ZnO nanopowders." *J. Mater. Sci. Lett*., Vol. 20, pp. 1381-1383.

Liu, Y., Liu, H., Chen, Z., Kadasala, N., Mao, C., Wang, Y., Zhang, Y., Liu, H., Liu, Y., Yang, J. and Yan, Y. (2014). "Effects of Ni concentration on structural, magnetic and optical properties of Ni-doped ZnO nanoparticles." *Journal of Alloys and Compounds*, Vol. 604, pp. 281-285.

Martinson, A. B. F., Elam, J. W., Hupp, J. T. and Pellin, M. J. (2007). "ZnO Nanotube Based Dye-Sensitized Solar Cells." *Nano Lett*., Vol. 7, No. 8, pp. 2183–2187.

Mitra, P., Chatterjee, A. P. and Maiti, H. S. (1998). "ZnO thin film sensor." *Mater. Lett*., Vol. 35, pp. 33-38.

Motaung, D. E., Kortidis, I., Papadaki, D., Nkosi, S. S., Mhlongo, G. H., Wesley-Smith, J., Malgas, G. F., Mwakikunga, B. W., Coetsee, E., Swart, H. C., Kiriakidis, G. and Ray, S. S. (2014). "Defect-induced magnetism in un-doped and Mn-doped wide band gap Zinc oxide grown by aerosol spray pyrolysis." *Appl. Surf. Sci*., Vol. 311, pp. 14-26.

Pearton, S. J., Norton, D. P., Ip, K., Heo, Y. W., Steiner, T. (2005). "Recent progress in processing and properties of ZnO." *Prog. Mater. Sci*., Vol. 50, No. 3, pp. 293–340.

Raja, K., Ramesh, P. S. and Geetha, D. (2014). "Synthesis, structural and optical properties of ZnO and Ni-doped ZnO hexagonal nanorods by Co-precipitation method." *Spectrochimica Acta Part A: Molecular and Biomolecular Spectroscopy*, Vol. 120, pp. 19-24.

Rajakarthikeyan, R. K., and Muthukumaran, S. (2017). "Investigation of microstructure, electrical and photoluminescence behaviour of Ni-doped $Zn_{0.96}Mn_{0.04}O$ nanoparticles: Effect of Ni concentration." *Opt. Mater*., Vol. 69, pp. 382-391.

Rana, A. K., Bankar, P., Kumar, Y., More, M. A., Late, D. J., Shirage, P. M. (2016). "Synthesis of Ni-doped ZnO nanostructures by low-temperature wet chemical method and their enhanced field emission properties." *RSC Adv*., Vol. 6, pp. 104318-104324.

Romeiro, F. C., Marinho, J. Z., Lemos, S. C. S., de Moura, A. P., Freire, P. G., da Silva, L. F., Longo, E., Munoz, R. A. A. and Lima, R. C. (2015). "Rapid synthesis of Co, Ni co-doped ZnO nanoparticles: Optical and electrochemical properties." *Journal of Solid State Chemistry*, Vol. 230, pp. 343-349.

Saito, N., Haneda, H., Sekiguchi, T., Ohashi, N., Sakaguchi, I. and Koumoto, K. (2002). "Low-Temperature Fabrication of Light-Emitting Zinc Oxide Micropatterns Using Self-Assembled Monolayers." *Adv. Mater*., Vol. 14, No. 6, pp. 418-421.

Samanta, A., Goswami, M. N. and Mahapatra, P. K. (2018). "Magnetic and electric properties of Ni-doped ZnO nanoparticles exhibit diluted magnetic semiconductor in nature." *Journal of Alloys and Compounds*, Vol. 730, pp. 399-407.

Schneider, J. J., Hoffmann, R. C., Engstler, J., Klyszcz, A., Erdem, E., Jakes, P., Eichel, R. A., Pitta-Bauermann L. and Bill, J. (2010). "Synthesis, characterization, defect chemistry, and FET properties of microwave-derived nanoscaled zinc oxide." *Chem. Mater*., Vol. 22, No. 2203-2212.

Shoushtari, M. Z., Poormoghadam, A. and Farbod, M. (2017). "The size dependence of the magnetic properties of ZnO and $Zn_{1-x}Ni_xO$ nanoparticles." *Materials Research Bulletin*, Vol. 88, pp. 315-319.

Srinet, G., Kumar, R. and Sajal, V. (2013). "Structural, optical, vibrational, and magnetic properties of sol-gel derived Ni doped ZnO nanoparticles." *Journal of Applied Physics*, Vol. 114, pp. 033912.

Toloman, D., Mesaros, A., Popa, A., Raita, O., Silipas, T. D. B., Vasile, S., Pana, O. and Giurgiu, L. M. (2013). "Evidence by EPR of ferromagnetic phase in Mn-doped ZnO nanoparticles annealed at different temperatures." *Journal of Alloys and Compounds*, Vol. 551, pp. 502-507.

Vignesh, K., Rajarajan, M. and Suganthi, A. (2014). "Visible light assisted photocatalytic performance of Ni and Th co-doped ZnO nanoparticles for the degradation of methylene blue dye." *J. Ind. Eng. Chem*., Vol. 20, No. 5, pp. 3826-3833.

Vijayaprasath, G., Murugan, R., Asaithambi, S., Sakthivel, P., Mahalingam, T., Hayakawa, Y. and Ravi G. (2016). "Structural and magnetic behavior of Ni/Mn co-doped ZnO nanoparticles prepared by co-precipitation method." *Ceramics International*, Vol. 42, pp. 2836-2845.

Xu, K., Liu, C., Chen, R., Fang, X., Wu, X. and Liu, J.

(2016). "Structural and room temperature ferromagnetic properties of Ni doped ZnO nanoparticles via low-temperature hydrothermal method." *Physica B*, Vol. 502, pp. 155-159.

Yildirimcan, S., Ocakoglu, K., Erat, S., Emen, F. M., Repp, S. and Erdem, E. (2016). "The effect of growing time and Mn concentration on the defect structure of ZnO nanocrystals: X-ray diffraction, infrared and EPR spectroscopy." *RSC Adv.*, Vol. *6*, No. 45, pp. 39511–39521.